The role of thermodynamic phase shifts in cloud optical depth variations with temperature

Ivy Tan[1,2], **Lazaros Oreopoulos**[1] **and Nayeong Cho**[1,2]

[1]Earth Sciences Division, NASA GSFC, Greenbelt, Maryland, USA.
[2]Universities Space Research Association, Columbia, Maryland, USA.

Key Points:

- Results of a novel method suggest that phase shifts dominate mid-latitudinal cloud optical depth increases with temperature compared to liquid and ice processes.
- The contribution of phase shifts to cloud optical depth variations with temperature is not strongly sensitive to dynamics.
- Thermodynamic phase shifts contribute more to increases in cloud optical depth with temperature during colder seasons.

Corresponding author: Ivy Tan, `ivy.tan@nasa.gov`

Abstract

We present a novel method that identifies the contributions of thermodynamic phase shifts and processes governing supercooled liquid and ice clouds to cloud optical depth variations with temperature using MODIS observations. Our findings suggest that thermodynamic phase shifts outweigh the net influence of processes governing supercooled liquid and ice clouds in causing increases in mid-latitudinal cold cloud optical depth with temperature. Cloud regime analysis suggests that dynamical conditions appear to have less influence on the contribution of thermodynamic phase shifts to cloud optical depth variations with temperature. Thermodynamic phase shifts also contribute more to increases in cloud optical depth during colder seasons due to the enhanced optical thickness contrast between liquid and ice clouds. The results of this study highlight the importance of thermodynamic phase shifts in explaining cold cloud optical depth increases with temperature in the current climate and may elucidate their role in the cloud optical depth feedback.

1 Introduction

Clouds, covering an average of ∼67% of Earth's surface [*King et al.*, 2013], play a critical role in Earth's radiation balance mainly by increasing the global amount of reflected shortwave (SW) radiation by ∼46 $\mathrm{Wm^{-2}}$ and by reducing the amount of longwave (LW) terrestrial radiation emitted to space by ∼28 $\mathrm{Wm^{-2}}$, resulting in a net cooling of ∼18 $\mathrm{Wm^{-2}}$ [*Loeb et al.*, 2018]. While the net effect of clouds on the present-day radiation balance is to cool the planet on average, it remains unclear how changes in clouds will either amplify or damp the warming induced by increases in greenhouse gases through various feedback mechanisms. Some of these changes in cloud responses to greenhouse gas forcing occur on a relatively rapid timescale of a few weeks [*Andrews et al.*, 2012], while others are mediated by changes in the global mean surface temperature [*Stocker et al.*, 2013], and thus occur on much slower timescales. Disparate responses of the latter type, referred to as cloud feedback, have been identified to contribute the greatest uncertainty in Earth's changing energy budget [*Stocker et al.*, 2013] and therefore in climate projections.

Despite the large uncertainty in cloud feedback, robust features have emerged in climate models. There is a consensus among the fifth phase of the Cloud Model Intercomparison Project (CMIP5) models that the optical depth, τ of low-clouds in the extratropics robustly increases with warming [*Zelinka et al.*, 2012; *Ceppi et al.*, 2017]. Since an increase in τ increases the amount of sunlight reflected back to space, the increase in τ with temperature leads to a negative extratropical cloud optical depth feedback in the CMIP5 models. τ is a function of cloud water content and the vertical profile of effective radius. Early in situ aircraft measurements in the 1960s in the Soviet Union have noted that cold cloud liquid water content (LWC), and hence τ, increases with temperature [*Feigelson*, 1978]. Moist thermodynamic relationships can be invoked to explain this increase in cold cloud LWC. It has been shown that the amount of condensed water in saturated rising air parcels along a moist adiabat scales with the temperature derivative of the moist adiabat [*Betts and Harshvardhan*, 1987]. τ-temperature relationships derived from International Satellite Cloud Climatology Project (ISCCP) satellite observations have shown that increases in τ with temperature over cold continental clouds are in the range of those measured by *Feigelson* [1978], suggesting that an increase in adiabatic water content is potentially the primarily physical mechanism responsible for increases in τ with air temperature in cold continental clouds [*Tselioudis et al.*, 1992]. In contrast, the ISCCP observations have also revealed that τ decreases with temperature over the warmer tropics and subtropics. Thereafter, *Tselioudis et al.* [1998] confirmed that these τ-temperature relationships are consistent with those observed after CO_2 doubling in NASA's GISS climate model, although the model was found to exaggerate the increase (decrease) in τ with warming in the mid-latitudes (subtropics and tropics). An analysis of the models participating in phases 1 and 2 of the Cloud Feedback Model Intercomparison Project (CFMIP1 and CFMIP2) revealed that similarly to the GISS climate model, many other models generally exhibit the typical trait of overestimating cold and warm τ increases with temperature over both land and ocean [*Gordon and Klein*, 2014]. As *Tselioudis et al.* [1998], *Gordon and Klein* [2014] and *Terai et al.* [2016] have demonstrated, the fact that the τ-temperature relationships are well-correlated with the cloud optical depth feedback in response to CO_2 doubling in models implies that the τ-temperature relationships are timescale invariant and can thus act as an emergent constraint for the cloud optical depth feedback. However, a key obstacle hindering the establishment of an emergent constraint for the cloud optical depth feedback is the lack of a clear understanding of the dominant physical mechanisms that can explain the empirical relationship between τ-temperature relationships and the cloud optical depth feedback. Establishing the dominant physical mechanisms responsible for the empirical relationships is important as the empirical relationships can be fortuitous [*Klein and Hall*, 2015].

Aside from mechanisms primarily associated with changes in cloud water content, another physical mechanism that can explain changes in τ with temperature relates to changes in cloud particle effective radius. This mechanism is pertinent to mixed-phase clouds, i.e. clouds that are comprised of mixtures of supercooled liquid droplets and ice crystals. Thermodynamic phase shifts from ice to liquid hydrometeors in mixed-phase clouds occur as the atmosphere warms in what is known as the "cloud phase feedback" [*Mitchell et al.*, 1989; *Tsushima et al.*, 2006; *McCoy et al.*, 2014a; *Tan et al.*, 2016; *Frey and Kay*, 2017]. Since liquid droplets are typically more abundant and smaller in size compared to their solid counterparts [*Pruppacher and Klett*, 1997], shifts from the ice to liquid phase within mixed-phase clouds can increase τ due to the fact that extinction is inversely proportional to effective radius; therefore, for a fixed water content, τ increases (decreases) when ice (liquid) is replaced with liquid (ice). An increase in the availability of ice in mixed-phase clouds would therefore increase the potential for an ice-to-liquid transition, which could result in increased τ. Thermodynamic phase changes from liquid to ice, on the other hand, can also occur as a result of the Wegener-Bergeron-Findeisen process [*Wegener*, 1911; *Bergeron*, 1935; *Findeisen*, 1938], a process whereby ice crystals grow at the expense of surrounding liquid droplets when the ambient vapour pressure is greater than the saturation vapour pressure over ice and less than the saturation vapour pressure over liquid. Thermodynamic phase changes due to the WBF process occur on relatively fast timescales and generally act to decrease τ by replacing liquid droplets with ice crystals; a mixed-phase cloud can completely glaciate within hours, although they have been observed to exist for days or even weeks [*Morrison et al.*, 2012] depending on the local vertical updraft velocity, ice particle number concentration and LWC [*Korolev and Isaac*, 2003]. Nonetheless, the longer-term impact of the WBF process on the climatological partitioning of liquid and ice in mixed-phase clouds and climate may be substantial [*Tan and Storelvmo*, 2016; *Tan et al.*, 2016].

Here we present a novel method that takes advantage of Moderate Resolution Imaging Spectroradiometer (MODIS)'s ability to partition τ into contributions from liquid and ice clouds at the grid cell level to determine the role of thermodynamic phase shifts to changes in τ with temperatures relative to processes operating in liquid and ice clouds.

2 Dataset and Derivation

MODIS is a spectroradiometer that measures solar reflected and thermal emitted radiation at 36 spectral bands ranging in wavelength from 0.4 μm to 14.4 μm. MODIS operates on both the Terra platform, which is in a descending node that crosses the equator at 10:30 am local time and the Aqua platform, which is in an ascending node that crosses the equator at 1:30 pm local time. MODIS has a relatively wide swath of 2330 km (cross track) by 10 km (along track at nadir) that covers Earth's entire surface within two days. The derivation presented in this section involves MODIS-Aqua's level 3 daily gridded (1°) Collection 6 (C6) cloud optical and microphysical properties product [*Platnick et al.*, 2017] for the four-year time period extending from January 1, 2013 to December 31, 2016. Using this product, we have verified that to good approximation (Figure S1),

$$\overline{\ln \tau(T)} = k_i(T)\overline{\ln \tau_i(T)} + k_l(T)\overline{\ln \tau_l(T)}, \tag{1}$$

where ln is the natural logarithm, T is temperature (cloud-top temperature (CTT) in our analysis), k_i (k_l) is the number of ice (liquid) pixels divided by the total number of liquid and ice pixels within a 1° by 1° grid cell, and the overbars represent daily averages in a grid cell. Daytime τ retrievals are originally performed at 1 km resolution. The daytime τ retrievals require prior determination of the thermodynamic phase of the clouds [*Platnick et al.*, 2017], which is obtained by employing a voting methodology that takes into account the output of several phase determination tests in C6 [*Marchant et al.*, 2016]. The phase information is derived using a combination of visible, shortwave infrared and infrared channels, and the phase thresholds used in the daytime algorithm were optimized using collocated measurements from Cloud-Aerosol Lidar with Orthogonal Polarization (CALIOP) [*Winker et al.*, 2009]. Daytime-retrieved τ is then estimated using look-up tables derived from radiative transfer calculations [*Nakajima and King*, 1990]. Although the MODIS C6 product introduces partly cloudy and edge (collectively referred to as "PCL") pixels as a separate category, we did not include these pixels in our analysis as they are known to be of lower quality and have higher retrieval failure rates compared to the regular MODIS retrievals [*Platnick et al.*, 2017]. However, we note that this may potentially result in a systematic bias towards optically thicker clouds [*Platnick et al.*, 2017]. MODIS computes CTT from CTP via re-analysis profiles that relate atmospheric temperature to pressure. CTP is retrieved using two different methods depending on cloud height: for mid-level and high clouds the CO_2 slicing technique is employed; for low clouds (CTP $>$ 700 hPa) infrared brightness temperature is used.

Equation 1 can be rewritten as

$$\begin{aligned}\overline{\ln\tau(T)} &= k_i(T)\overline{\ln\tau_i(T)} + (1-k_i(T))\overline{\ln\tau_l(T)} \qquad (2)\\ &= k_i(T)\left(\overline{\ln\tau_i(T)} - \overline{\ln\tau_l(T)}\right) + \overline{\ln\tau_l(T)}. \qquad (3)\end{aligned}$$

Taking the temperature derivative of Equation 3 yields

$$\begin{aligned}\frac{d\overline{\ln\tau}}{dT} &= \tfrac{dk_i}{dT}\left(\overline{\ln\tau_i(T)} - \overline{\ln\tau_l(T)}\right) + k_i(T)\tfrac{d\overline{\ln\tau_i}}{dT} - k_i(T)\tfrac{d\overline{\ln\tau_l}}{dT} + \tfrac{d\overline{\ln\tau_l}}{dT} \qquad (4)\\ &= \tfrac{dk_i}{dT}\left(\overline{\ln\tau_i(T)} - \overline{\ln\tau_l(T)}\right) + k_i(T)\tfrac{d\overline{\ln\tau_i}}{dT} + k_l(T)\tfrac{d\overline{\ln\tau_l}}{dT}. \qquad (5)\end{aligned}$$

The first term on the right-hand side (RHS) of Equation 5 represents the contribution of thermodynamic phase shifts to variations in τ with temperature, and is the product of the rate of change in the fraction of ice cloud pixels with CTT and the difference in the mean logarithms of ice and liquid clouds. The second term on the RHS of Equation 5 represents the contribution of processes operating in ice clouds to variations in τ with temperature. The third term on the RHS of Equation 5 represents the contribution of processes operating in liquid clouds to $\frac{d\overline{\ln\tau}}{dT}$. The derivatives were computed by regressing the relevant daily gridded mean values on daily mean CTT values in 15°C temperature bins. Since mean grid values were used in the analysis, grid cells containing both high ice clouds and low liquid clouds could be mistaken for a middle-level cloud since cloud properties are averaged within each grid cell. To minimize such instances, the data were filtered to exclude grid cells where the standard deviation of CTT $>$ 5°C. The weighting factors multiplying the derivatives in the right-hand side of Equation 5 were computed as the mean of all values used in the regression that determined the derivative values. Since MODIS relies on measured reflectance for its retrievals of τ, data poleward of 55° were excluded from the analysis to avoid potential contamination from bright surfaces. Analysis of the statistics of solar zenith angle (SZA) within each of the 15°C temperature bins revealed very little variation in SZA between the temperature bins, suggesting that any τ biases due to SZA effects do not depend systematically on CTT. The main focus of this work is on the first term, i.e. the contribution of thermodynamic phase shifts to $\frac{d\ln\tau}{dT}$ in the current climate.

3 Results

The results of the decomposition method are presented in this section as plots of $\frac{d\ln\tau}{dT}$ variations with CTT. Each CTT value on the abscissa represents the mid-point of a 15°C temperature bin, over which the linear regressions were performed. The temperature bins overlap and their mid-points are separated by 2°C. Since the focus of this work is on the contribution of thermodynamic phase shifts to $\frac{d\ln\tau}{dT}$, the temperature range considered spans from the approximate homogeneous freezing temperature of −40°C to 0°C, above which water can only exist in liquid phase. A decomposition of variations in τ by climatic zone is presented first in Section 3.1. Subsequent analyses focus on the contribution of thermodynamic phase changes to variations in τ. The decomposition method is applied to various "cloud regimes" in Section 3.2 to determine the extent to which thermodynamic phase shifts change depending on the local dynamical conditions. Finally, the seasonal dependences of the phase shift term are presented in Section 3.3.

3.1 Decomposition of Cloud Optical Depth Variations with Temperature Driven by Latitude

The decomposition of τ variations with CTT following Equation 5 is plotted as a function of temperature for the mid-latitudes (35° to 55° in both hemispheres), subtropics (15° to 35° in both hemispheres) and tropics (15°S to 15°N) and shown separately over land and ocean in Figure 1. Values that are statistically significant (insignificant) at the 95% level, according to the F-test are denoted by open (closed) symbols. Although investigation of the physical processes responsible for the contribution of ice and liquid clouds to $\frac{d\ln\tau}{dT}$ (second and third terms on the RHS of Equation 5, respectively) is beyond the scope of this study, these terms are nevertheless shown to put the contribution of thermodynamic phase shifts to $\frac{d\ln\tau}{dT}$ (first term on the RHS of Equation 5) in context. Processes related purely to liquid clouds include but are not limited to changes in adiabatic water content, precipitation, cloud-top entrainment and other processes related to boundary-layer decoupling for low-clouds. Some processes related to ice clouds include precipitation, riming, ice nucleation and ice splintering.

We have verified that the sum of the three terms in the decomposition highly correlates (R$\sim$0.99) with $\frac{d \ln \tau}{dT}$ when computed using the MODIS daytime-retrieved total τ (i.e. the combined τ value that does not distinguish thermodynamic phase) for the various latitude bands (Figure S2). This shows that our method accurately decomposes $\frac{d \ln \tau}{dT}$.

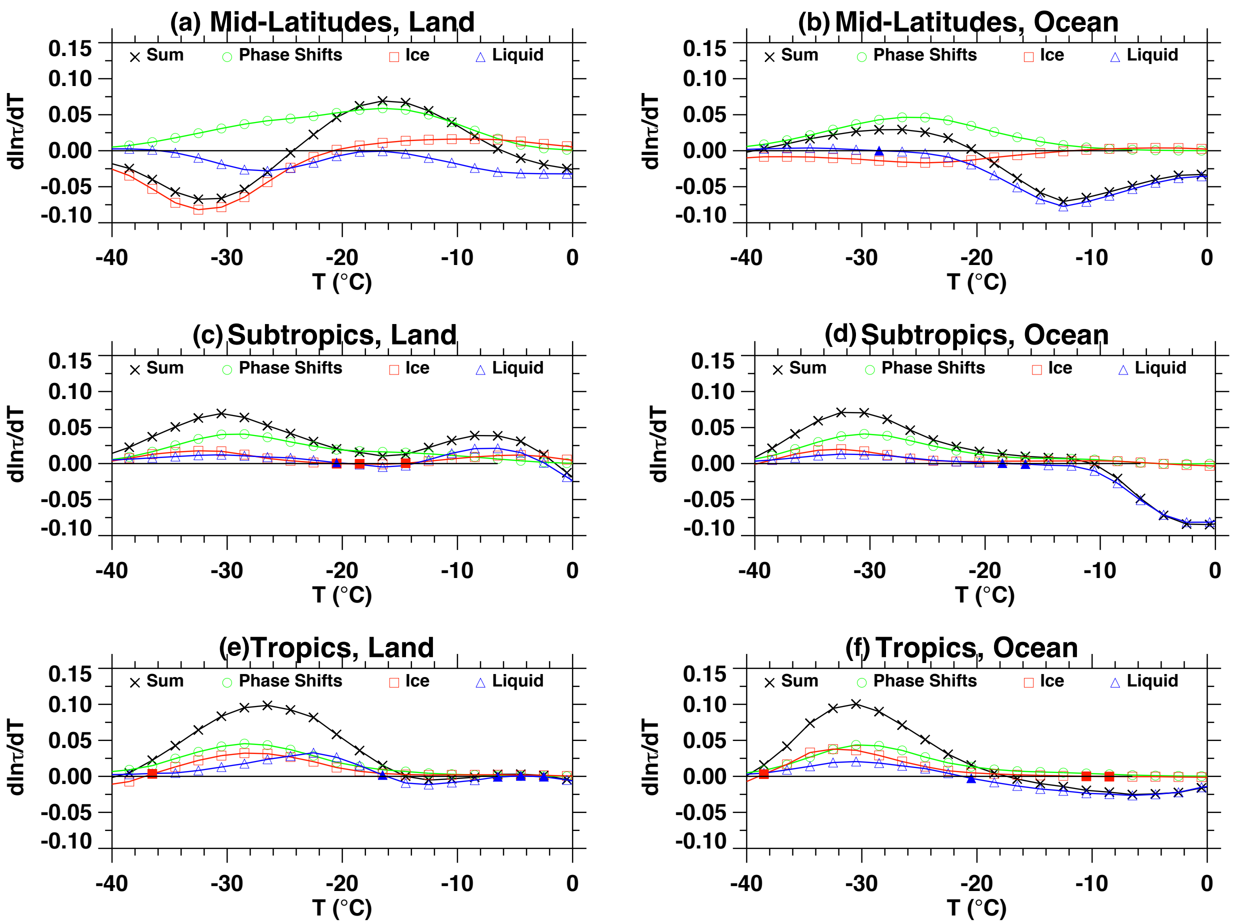

Figure 1. Decomposition of cloud optical depth variations with cloud-top temperature ($\frac{d \ln \tau}{dT}$) as a function of cloud-top temperature over (a) mid-latitude land, (b) mid-latitude ocean, (c) subtropical land, (d) subtropical ocean, (e) tropical land and (f) tropical ocean. Open (closed) symbols indicate values that are statistically significant (insignificant) at the 95% level according to the F-test.

It is evident from Figure 1 that the thermodynamic phase shift term is always positive. This contribution, represented by the first term on the right-hand side of Equation 5 is the product of two quantities that are usually negative: the difference in logarithmic means of τ in a grid cell is usually negative because of the inverse relationship between extinction and particle size previously discussed (typically causing $\overline{\ln \tau_l} > \overline{\ln \tau_i}$), while the derivative is also negative because the fraction of ice pixels decreases with temperature.

It is interesting to note that physical processes affecting liquid and ice clouds always cause τ to decrease with temperature between $-40°$C and $0°$C in the mid-latitudes, with the exception of ice cloud processes operating over relatively warmer temperatures over land in the mid-latitudes that cause small increases in τ with temperature. The fact that the thermodynamic phase shift term is the largest in magnitude of any term contributing to increases in cloud optical depth variations with temperature suggests that thermodynamic phase shifts are the main cause of increases in cloud optical depth with temperature in the mid-latitudes relative to physical processes affecting liquid and ice clouds. However, we note liquid cloud processes play a strong counterbalancing role by driving decreases in cloud optical depth variations with temperature.

A comparison of the sum of the decomposed terms, displayed in black in Figures 1a to d with Figure 4 in *Tselioudis et al.* [1992], who quantified $\frac{d \ln \tau}{dT}$ using 3-hour averages of ISCCP observations over the same regions in 280-km-wide areas reveals the same overall qualitative features. In particular, $\frac{d \ln \tau}{dT}$ is positive over land at colder temperatures but reverses to become negative at warmer temperatures. However, extension of patterns of $\frac{d \ln \tau}{dT}$ to temperatures colder than $-24°$C over land reveals that $\frac{d \ln \tau}{dT}$ becomes negative once again. Over the ocean, $\frac{d \ln \tau}{dT}$ is negative and becomes positive below a threshold temperature. It is important to note, however, that a direct comparison with *Tselioudis et al.* [1992] is not possible due to fundamental differences in the methodology used. Namely, while *Tselioudis et al.* [1992] excluded all clouds with tops outside the 680 to 800 hPa range, we use in our analysis all clouds within a $1°$ by $1°$ grid cell as long as the standard deviation of CTT $< 5°$C. Another key difference between the two methods is the type of temperature used; while *Tselioudis et al.* [1992] used mean (averaged horizontally and vertically) air temperature in their analysis of low-clouds, this analysis uses mean (averaged horizontally only) CTT. Similarly, a comparison between our Figure 1 and Figure 1 in *Gordon and Klein* [2014] may not be appropriate since *Gordon and Klein* [2014] consider only low-clouds in models.

In contrast to the mid-latitudes, the contributions of liquid and ice cloud processes to $\frac{d \ln \tau}{dT}$ tend to be positive at colder temperatures but decreases at warmer temperatures until they become negative in the subtropics and tropics. The positive contribution of thermodynamic phase shifts to $\frac{d\ln\tau}{dT}$ is always greater than that of the individual contributions of liquid and ice cloud processes in these climatic zones.

3.2 Contribution of Thermodynamic Phase Shifts to Cloud Optical Depth Variations with Temperature by Cloud Regime

Correlation coefficients for the linear regression between $\ln\tau$ and CTT in the analysis above were typically $\sim$0.3 or greater. The lack of a stronger correlation between $\ln\tau$ and temperature indicates that factors other than temperature also play an important role in influencing cloud optical depth. Dynamical influences such as vertical updraft velocity and wind shear are examples of local dynamical variables that can impact cloud optical depth variations. One way to account for the influence of local dynamical conditions is to employ the cloud regime (CR) approach for classifying grid cell cloudiness. First coined "weather states" [*Jakob and Tselioudis*, 2003; *Rossow et al.*, 2005], these cloud classes were first derived using k-means clustering on ISCCP observations to group clouds by their optical depth and CTP covariations. The development of other CRs followed [*Gordon et al.*, 2005; *Tan et al.*, 2013; *Mason et al.*, 2014; *Oreopoulos et al.*, 2014].

We apply the decomposition method to the MODIS cold-CRs to determine the extent to which cloud optical depth variations with temperature are influenced by the dynamical state of the atmosphere. For a detailed description of the original derivation of the MODIS regimes, the reader is referred to *Oreopoulos et al.* [2014]. Although cloud regimes were derived using k-means clustering applied to 12 years (December 2002 to November 2014) of global daily, level 3, gridded (1°) CTP-τ histograms from both MODIS onboard Aqua and Terra [*Oreopoulos et al.*, 2016], only cloud regime occurrences from MODIS onboard Aqua were used in our analysis consistently with the remaining analysis in this paper. Of the CRs of [*Oreopoulos et al.*, 2016], only CRs 2 to 6 and 12 were considered in the analysis. CRs 2 to 6 are either dominated by the ice phase or contain substantial amounts of ice, while CR 12 contains no characteristic cloud types, but rather consists of cloud types found at different latitudes with small cloud fraction. Although CR 1 contains a large amount of ice clouds, cloud occurrences were too infrequent to apply the decomposition method. For presentation purposes, the decomposition method was applied to groups of CRs that were similar as follows: CRs 2 and 3 are mostly comprised of optically thick high clouds generated by tropical and frontal convection, and CRs 4 to 6 are mostly mid-level clouds generated in the storm tracks.

The ability of the CRs to group clouds by the uniqueness of their meteorological environment is supported by their distinctness in large-scale vertical velocity at 500 hPa (ω_{500}) from MERRA-2 Reanalysis, as shown by Figure 3 in *Oreopoulos et al.* [2016]. Statistical values of ω_{500} for CRs 2–6 and 12 used in our analysis are substantially different from one another, with some of the CRs having lower mean and median values clearing the lower quartile for the CRs having the higher mean and median values. CR12 is in a category of its own with a negative ω_{500} value, signifying that it primarily occurs in regions of descending motion. Since large-scale vertical velocity even by itself is a differentiator of dynamical conditions, we may conclude that CRs 2–6 and 12 considered in our study occur in sufficiently different dynamical regimes.

The contributions of thermodynamic phase shifts to $\frac{d\ln\tau}{dT}$ resulting from application of the decomposition method to the MODIS Aqua cold-cloud regimes are shown in Figure 2. When regressions were performed on data for individual cloud regimes, the correlation coefficients were higher ($\sim$0.4 or greater) than in our previous analysis that did not discriminate for different cloud classes. The results suggest that despite categorizing the cloud types by similarity in dynamical conditions, patterns of cloud optical depth variations with temperature largely remain unchanged. The fact that contributions of thermodynamic phase shifts to $\frac{d\ln\tau}{dT}$ are largely independent of CR implies that thermodynamic influences on $\frac{d\ln\tau}{dT}$ outweigh dynamical influences.

3.3 Seasonality of Cloud Optical Depth Variations due to Thermodynamic Phase Shifts

In this section, the impact of thermodynamic phase shifts on $\frac{d\ln\tau}{dT}$ is examined in the subtropics and midlatitudes as a function of season. The tropics have been excluded from the analysis due to much smaller seasonal variations in temperature. This is worth investigating because the altitude-temperature relationship varies with season. For this analysis, data from September 1, 2002 to Dec. 31, 2017 were used. The first row of Figure 3 shows $\frac{d\ln\tau}{dT}$ due to thermodynamic phase shifts in both hemispheres.

Within a certain temperature range, the contribution of thermodynamic phase shifts to increases in cloud optical depth with temperature tends to be largest in winter and

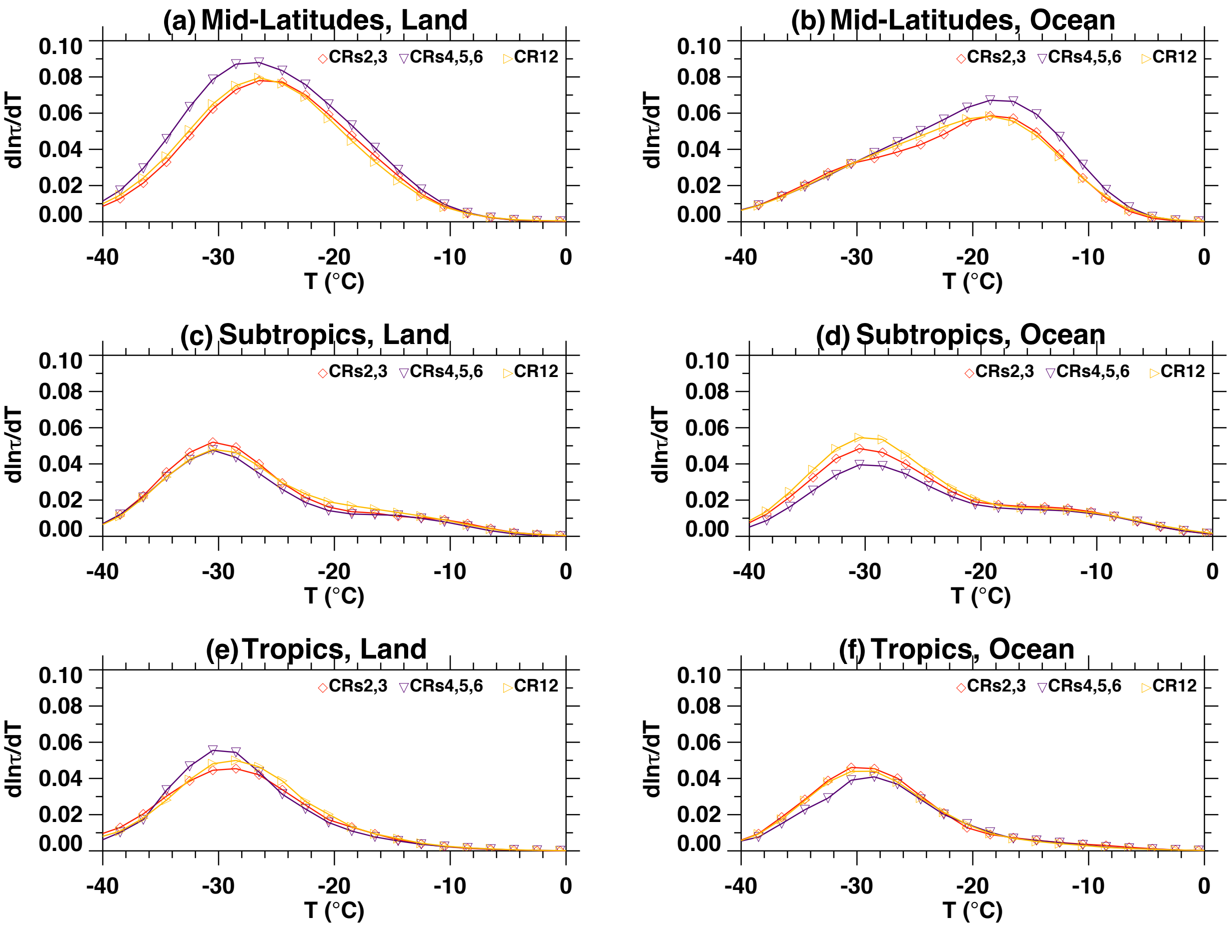

Figure 2. The contributions of thermodynamic phase shifts to cloud optical depth variations with temperature over (a) mid-latitude land, (b) mid-latitude ocean, (c) subtropical land, (d) subtropical ocean, (e) tropical land and (f) tropical ocean applied to 4 CR groups with large proportions of ice.

decreases with warmer seasonal temperatures over both land and ocean in both hemispheres. To better understand the observed pattern, we plot the subterms $\overline{\ln \tau_i} - \overline{\ln \tau_l}$ and $\frac{dk_i}{dT}$ (second and third rows of Figure 3, respectively).

Inspection of these two subterms reveals an interesting behaviour — $\frac{dk_i}{dT}$ determines the peak contribution of the phase shift term, while $\overline{\ln \tau_i} - \overline{\ln \tau_l}$ determines its relative magnitude. This suggests that the seasonal strength of thermodynamic phase shifts is determined mainly by the average optical depth difference between ice and liquid clouds, and the temperature at which the largest shift occurs is determined by the peak rate at which this difference in τ is created. The explanation for why $\frac{dk_i}{dT}$ is consistently neg-

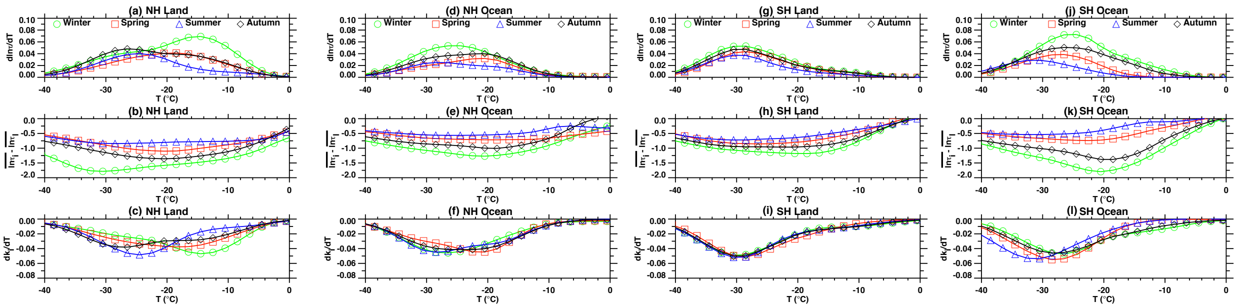

Figure 3. The contribution of thermodynamic phase shifts to cloud optical depth variations with temperature as a function of temperature in the 25°N to 55°N latitude band broken down by season over (a) land and (d) ocean in the Northern Hemisphere and (g) land and (h) ocean in the Southern Hemisphere. The two terms, $\overline{\ln\tau_i} - \overline{\ln\tau_l}$ and $\frac{dk_i}{dT}$ that when multiplied yield the thermodynamic phase shift term are shown for the corresponding regions in each column in the second and third row, respectively. Winter (for NH: December, January, February; for SH: June, July, August), spring (for NH: March, April, May; for SH: September, October, November), summer (for NH: June, July, August; for SH: December, January, February) and fall (for NH: September, October, November; for SH: March, April, May).

ative is well-known — the likelihood that ice crystals occur along with supercooled liquid droplets increases as temperature decreases (e.g. *Pruppacher and Klett* [1997]; *Murray et al.* [2012] and as observed by satellite instruments [*Hu et al.*, 2010; *McCoy et al.*, 2014b; *Tan et al.*, 2014]). Negative $\overline{\ln\tau_i}-\overline{\ln\tau_l}$ values are consistent with the cloud phase feedback. In other words, ice-to-liquid transitions in the cloud phase feedback result in $\tau_i<\tau_l$ because extinction is smaller for ice compared to liquid clouds for a given water content. It generally appears that $\overline{\ln\tau_i}-\overline{\ln\tau_l}$ is most negative in boreal and austral winter, and is followed by autumn, spring and summer.

One may speculate that the seasonal and hemispheric differences in $\frac{dk_i}{dT}$ and $\overline{\ln\tau_i}-\overline{\ln\tau_l}$ within the fixed temperature ranges shown in Figure 3 may be related to the competing role of ice-nucleating particles (INPs) and cloud condensation nuclei (CCN) in determining cloud phase partitioning and therefore τ of mixed-phase clouds. If a short-term cloud phase feedback indeed plays a role in the observed patterns, then more positive contributions of thermodynamic phase shifts to $\frac{d\ln\tau}{dT}$ would be expected if more ice in clouds is available for ice-to-liquid transitions, for example, through the enhanced availability of INPs relative to CCN. Clouds of the same CTT are closer to the surface in the winter and consequently their chances of being exposed to relative rare INPs [*Murray et al.*, 2012] increase. We hypothesize that greater exposure to INPs creates more ice clouds at temperatures where they would otherwise be supercooled, thus increasing the likelihood for ice-to-liquid transitions, and therefore a larger phase shift term. We note that the peak in $\frac{dk_i}{dT}$ occurs at lower temperatures in the Southern Hemisphere, which includes the Southern Ocean region. This is consistent with the previous studies that have shown that the Southern Ocean is abundant in supercooled liquid clouds and relatively INP-free [*Tan et al.*, 2014; *Bodas-Salcedo et al.*, 2016; *Vergara-Temprado et al.*, 2018]. However, we note that the concentration, types and altitude of occurrence of INPs and CCN differ markedly between the Southern and Northern Hemispheres [*Andreae and Rosenfeld*, 2008; *Atkinson et al.*, 2013; *Cziczo et al.*, 2013; *Tan et al.*, 2014; *Wilson et al.*, 2015; *McCoy et al.*, 2015; *DeMott et al.*, 2016; *Vergara-Temprado et al.*, 2018], and that although our general knowledge of the impact of aerosols on mixed-phase clouds has greatly improved over time with the availability of improved observations, aerosol effects on mixed-phase clouds still remain uncertain [*Storelvmo*, 2017]. This uncertainty currently precludes a conclusive explanation for the observed patterns in Figure 3.

4 Discussion and Conclusions

This study introduces a novel method to decompose spatiotemporal cloud optical depth variations with temperature into contributions from thermodynamic phase shifts and processes exclusive to liquid and ice clouds using observations of liquid and ice cloud optical depth retrieved by MODIS onboard the Aqua satellite. The focus of this study is on thermodynamic phase shifts and therefore accounts for all clouds as long as they exhibit moderate subgrid cloud top variations within ∼100 km scales. This contrasts with previous studies that have considered only low, mostly liquid-containing clouds, where thermodynamic phase shifts are limited [*Tselioudis et al.*, 1992, 1998; *DelGenio and Wolf*, 2000; *Gordon and Klein*, 2014; *Terai et al.*, 2016].

The main conclusions of this study are threefold. The first main conclusion is that the decomposition method suggests that increases in τ with CTT in the mid-latitudes (35° to 55°) are due to thermodynamic phase shifts and that processes exclusive to liquid and ice clouds act to either decrease or slightly increase τ with CTT. This finding suggests that the increase in $\frac{d\ln\tau}{dT}$ potentially arising from increases in adiabatic water content in the mid-latitudes in low-clouds [*Tselioudis et al.*, 1992; *Gordon and Klein*, 2014; *Terai et al.*, 2016] either does not extend to all clouds or is outweighed by other processes operating in liquid clouds. The second main conclusion is that dynamical conditions do not appear to be of primary importance for thermodynamic phase shifts to $\frac{d \ln \tau}{dT}$. This conclusion is drawn from the fact that the general pattern of the contribution of the phase shift term remained similar regardless of CR. The third main conclusion is that the contribution of thermodynamic phase shifts to $\frac{d \ln \tau}{dT}$ is larger during colder seasons. At what temperature range the maximum contribution of the phase shift term occurs is determined by the rate of change of the occurrence of ice clouds with temperature. The largest contribution of the phase shift term generally occurs during winter because it contains liquid clouds that are optically thicker than ice clouds on average within a fixed temperature range. This is consistent with the cloud phase feedback and we hypothesize that if a higher proportion of ice clouds is made available due to closer proximity to surface sources of INPs for a given temperature during the colder seasons, then the potential for ice-to-liquid transitions is enhanced, which would lead to a positive $\frac{d \ln \tau}{dT}$ derivative in a fixed temperature range.

Although the method presented here is able to determine the contribution of thermodynamic phase shifts to cold cloud optical depth variations with temperature, the main limitation of this study is its inability to account for the influence of geometrical thickness variations on τ variations due to the unavailability of such information from a passive instrument such as MODIS. Cloud physical thickness was shown to play an important role in determining how τ varies with temperature in modelling studies [*Tselioudis et al.*, 1998; *Gordon and Klein*, 2014] and in a study using active ground-based observations in the Southern Great Plains [*DelGenio and Wolf*, 2000]. Another limitation of this study is that MODIS's cloud phase retrievals tend to be cloud-top biased and it may therefore be missing occurrences of low liquid clouds underlying high ice clouds, thus making phase assignment ambiguous in those cases.

Ultimately, the goal is to determine the role of thermodynamic phase shifts in the long-term cloud optical depth feedback that occurs in response to global warming. Unfortunately, the relatively short current record from satellite observations precludes a direct calculation of the long-term cloud optical depth feedback and thus the findings of this study may not directly relate to the cloud optical depth feedback problem, although it may serve as an emergent constraint. An essential part of future work should focus on determining how cloud optical depth variations with cloud-top temperature relate to changes in surface-temperature.

Acknowledgments

Observations retrieved from MODIS are available online at NASA's LAADS website (https://ladsweb.modaps.eosdis.nasa.gov). This work was supported by the NASA Postdoctoral Program at NASA GSFC administered by University Space Research Association under contract with NASA. The authors thank Chen Zhou for helpful contributions and discussions while he was at Lawrence Livermore National Laboratory, and Kerry G. Meyer at NASA GSFC for helpful discussions.

References

Andreae, M. O., and D. Rosenfeld (2008), Aerosol-cloud-precipitation interactions. part 1. the nature and sources of cloud-active aerosols, *Earth Science Reviews*, *89*, 13–41.

Andrews, T., J. M. Gregory, P. M. Forster, and M. J. Webb (2012), Cloud adjustment and its role in CO_2 radiative forcing and climate sensitivity: A review, *Surveys in Geophysics*, *33*, 619–635.

Atkinson, J. D., B. J. Murray, M. T. Woodhouse, T. F. Whale, K. J. Baustian, K. S. Carslaw, S. Dobbie, D. O'Sullivan, and T. L. Malkin (2013), The importance of feldspar for ice nucleation by mineral dust in mixed-phase clouds, *Nature*, *498*, 355–358.

Bergeron, T. (1935), On the physics of clouds and precipitation, *Procès Verbaux de l'Association de Météorologie*, (156–178).

Betts, A. K., and Harshvardhan (1987), Thermodynamic constraint on the cloud liquid water feedback in climate models, *J. Geophys. Res.*, *92D*, 8483–8485.

Bodas-Salcedo, A., P. G. Hill, K. Furtado, K. D. Williams, P. R. Field, J. C. Manners, P. Hyder, and S. Kato (2016), Large contribution of supercooled liquid clouds to the solar radiation budget of the southern ocean, *J. Clim.*, *29*, 4213–4228.

Ceppi, P., F. Brient, M. D. Zelinka, and D. L. Hartmann (2017), Cloud feedback mechanisms and their representation in global climate models, *WIREs Clim. Change*, *e465*.

Cziczo, D. J., K. D. Froyd, C. Hoose, E. J. Jense, M. Diao, M. A. Zondlo, J. B. Smith, C. H. Twohy, and D. M. Murphy (2013), Clarifying the dominant sources and mechanisms of cirrus cloud formation, *Science*, *340*, 1320–1324.

DelGenio, A. D., and A. B. Wolf (2000), The temperature dependence of the liquid water path of low clouds in the southern great plains, *J. Clim.*, *13*, 3465–3486.

DeMott, P. J., T. C. J. Hill, C. S. McCluskey, K. A. Prather, D. B. Collins, R. C. Sullivan, M. J. Ruppel, R. H. Mason, V. E. Irish, T. Lee, C. Y. Hwang, T. S. Rhee, J. R. Snider, G. R. McMeeking, S. Khaniyala, E. R. Lewis, J. J. B. Wentzell, J. Abbatt, C. Lee, C. M. Sultana, A. P. Ault, J. L. Axson, M. D. Martinez, I. Venero, G. Santos-Figueroa, M. D. Stokes, G. B. Deane, O. L. Mayol-Bracero, V. H. Grassian, T. H. Bertram, A. K. Bertram, B. F. Moffett, and G. D. Franc (2016), Sea spray aerosol as a unique source of ice nucleating particles, *Proc. Natl. Acad. Sci.*, *113*, 5797–5803.

Feigelson, E. M. (1978), Preliminary radiation model of a cloudy atmosphere. part I: Structure of clouds and solar radiation, *Beitr. Phys. Atmos.*, *51*, 203–229.

Findeisen, W. (1938), Die kolloidmeteorologischen vorgänge bei der niederschlagsbildung, *Meteorol. Zeitschrift*, *55*, 121–133.

Frey, W. R., and J. E. Kay (2017), The influence of extratropical cloud phase and amount feedbacks on climate sensitivity, *Clim. Dyn.*, (1–20).

Gordon, N. D., and S. A. Klein (2014), Low-cloud optical depth feedback in climate models, *J. Geophys. Res.*, *119*, 6052–6065.

Gordon, N. D., J. R. Norris, C. P. Weaver, and S. A. Klein (2005), Cluster analysis of cloud regimes and characteristic dynamics of midlatitude synoptic systems in observations and a model, *J. Geophys. Res.*, *110*(D15).

Hu, Y., S. Rodier, K.-M. Xu, W. Sun, J. Huang, B. Lin, P. Zhai, and D. Josset (2010), Occurrence, liquid water content, and fraction of supercooled water clouds from combined CALIOP/IIR/MODIS measurements, *J. Geophys. Res.*, *115*(D00H34).

Jakob, C., and G. Tselioudis (2003), Objective identification of cloud regimes in the tropical western pacific, *Geophys. Res. Lett.*, *30*, 2082.

King, M. D., S. Platnick, W. P. Menzel, S. A. Ackerman, and P. A. Hubanks (2013), Spatial and temporal distribution of clouds observed by modis onboard the terra and aqua satellites, *IEEE Transactions on Geoscience and Remote Sensing*, *51*(3826–3852).

Klein, S. A., and A. Hall (2015), Emergent constraints for cloud feedbacks, *Curr. Clim. Change Rep.*, *1*, 276–287.

Korolev, A. V., and G. Isaac (2003), Phase transformation of mixed-phase clouds, *Quat. J. R. Meteor. Soc.*, *129*, 19–38.

Loeb, N. G., D. R. Doelling, H. Wang, W. Su, C. Nguyen, J. G. Corbett, L. Liang, C. Mitrescu, F. G. Rose, and S. Kato (2018), Clouds and the earth's radiant energy system (CERES) energy balanced and filled (EBAF) top-of-atmosphere (TOA) edition-4.0 data product, *J. Clim.*, *31*, 895–918.

Marchant, B., S. Platnick, K. Meyer, G. T. Arnold, and J. Riédi (2016), MODIS collection 6 shortwave-derived cloud phase classification algorithm and comparisons with CALIOP, *Atm. Meas. Tech.*, *9*, 1587–1599.

Mason, S., C. Jakob, A. Protat, and J. Delanoë (2014), Characterizing observed midtopped cloud regimes associated with southern ocean shortwave radiation biases, *J. Clim.*, *27*, 6189–6203.

McCoy, D. T., D. L. Hartmann, and D. P. Grosvenor (2014a), Observed southern ocean cloud properties and shortwave reflection. part ii: Phase changes and low cloud feedback, *J. Clim.*, *27*, 8858–8868.

McCoy, D. T., D. L. Hartmann, and D. P. Grosvenor (2014b), Observed southern ocean cloud properties and shortwave reflection. part i: Calculation of SW flux from observed cloud propertie, *J. Clim.*, *27*, 8836–8857.

McCoy, D. T., S. M. Burrows, R. Wood, D. P. Grosvenor, S. M. Elliott, P. L. Ma, P. J. Rasch, and D. L. Hartmann (2015), Natural aerosols explain seasonal and spatial patterns of southern ocean cloud albedo, *Science Advances*, *1*, e1500,157.

Mitchell, J. F. B., C. A. Senior, and W. J. Ingram (1989), CO_2 and climate: a missing feedback, *Nature*, *341*, 132–134.

Morrison, H., G. de Boer, G. Feingold, J. Harrington, M. D. Shupe, and K. Sulia (2012), Resilience of persistent arctic mixed-phase clouds, *Nature Geoscience*, *5*(1), 11–17.

Murray, B. J., E. O'Sullivan, J. D. Atkinson, and M. E. Webb (2012), Ice nucleation by particles immersed in supercooled cloud droplets, *Chem. Soc. Rev.*, *41*, 6519–6554.

Nakajima, T., and M. D. King (1990), Determination of the optical thickness and effective particle radius of clouds from reflected solar radiation measurements. part i: Theory, *J. Atmos. Sci.*, *47*, 1878–1893.

Oreopoulos, L., N. Cho, D. Lee, S. Kato, and G. J. Huffman (2014), An examination of the nature of global modis cloud regimes, *J. Geophys. Res.*, *119*, 8362–8383.

Oreopoulos, L., N. Cho, D. Lee, and S. Kato (2016), Radiative effects of global MODIS cloud regimes, *J. Geophys. Res.*, *121*, 2299–2317.

Platnick, S., K. G. Meyer, M. D. King, G. Wind, N. Amarasinghe, B. Marchant, G. T. Arnold, Z. Zhang, P. A. Hubanks, R. E. Holz, P. Yang, W. L. Ridgway, and J. Riédi (2017), The MODIS cloud optical and microphysical products: Collection 6 updates and examples from terra and aqua, *IEEE Transactions on Geoscience and Remote Sensing*, *55*, 502–525.

Pruppacher, H. R., and J. D. Klett (1997), *Microphysics of clouds and precipitation*, 2 ed., Kluwer Academic Publishers.

Rossow, W. B., G. Tselioudis, A. Polak, and C. Jakob (2005), Tropical climate described as a distribution of weather states indicated by distinct mesoscale cloud property mixtures, *Geophys. Res. Lett.*, *32*, L21,812.

Stocker, T. F., D. Qin, and G.-K. P. *et al.* (2013), *Technical summary: Climate change 2013: The physical science basis. Fifth assessment report of the intergovernmental panel on climate change.*

Storelvmo, T. (2017), Aerosol effects on climate via mixed-phase and ice clouds, *Annual Review of Earth and Planetary Sciences*, *45*, 199–222.

Tan, I., and T. Storelvmo (2016), Sensitivity study on the influence of cloud microphysical parameters on mixed-phase cloud thermodynamic phase partitioning in CAM5, *J. Atm. Sci.*, *73*, 709–728.

Tan, I., T. Storelvmo, and Y.-S. Choi (2014), Spaceborne lidar observations of the ice-nucleating potential of dust, polluted dust, and smoke aerosols in mixed-phase clouds, *J. Geophys. Res.*, *119*, 6653–6665.

Tan, I., T. Storelvmo, and M. D. Zelinka (2016), Observational constraints on mixed-phase clouds imply higher climate sensitivity, *Science*, *352*, 224–227.

Tan, J., C. Jakob, and T. P. Lane (2013), On the identification of the large-scale properties of tropical convection using cloud regimes, *J. Clim.*, *26*, 6618–6632.

Terai, C. R., S. A. Klein, and M. D. Zelinka (2016), Constraining the low-cloud optical depth feedback at middle and high latitudes using satellite observations, *J. Geophys. Res.*, *121*, 9696–9716.

Tselioudis, G., W. B. Rossow, and D. Rind (1992), Global patterns of cloud optical thickness variation with temperature, *J. Clim.*, *5*, 1484–1495.

Tselioudis, G., A. D. D. Genio, W. Kovari, and M.-S. Yao (1998), Temperature dependence of low cloud optical thickness in the GISS GCM: contributing mechanisms and climate implications, *J. Clim.*, *11*, 3268–3281.

Tsushima, Y., S. Emori, T. Ogura, M. Kimoto, M. J. Webb, K. D. Williams, M. A. Ringer, B. J. Soden, B. Li, and N. Andronova (2006), Importance of the mixed-phase cloud distribution in the control climate for assessing the response of clouds to carbon dioxide increase: a multi-model study, *Clim. Dyn.*, *27*, 113–126.

Vergara-Temprado, J., A. K. Miltenberger, K. Furtado, D. P. Grosvenor, B. J. Shipway, A. A. Hill, J. M. Wilkinson, P. R. Field, B. J. Murray, and K. S. Carslaw (2018), Strong control of southern ocean cloud reflectivity by ice-nucleating particles, *Proc. Natl. Acad. Sci.*, *115*, 2687–2692.

Wegener, A. (1911), *Thermodynamik der Atmosphäre*, JA Barth.

Wilson, T. W., L. A. Ladino, P. A. Alpert, M. N. Breckels, I. M. Brooks, J. Browse, S. M. Burrows, K. S. Carslaw, J. A. Huffman, C. Judd, W. P. Kilthau, R. H. Mason, G. McFiggans, L. A. Miller, J. J. Nájera, E. Polishchuk, S. Rae, C. L. Schiller, M. Si, J. V. Temprado, T. F. Whale, J. P. S. Wong, O. Wurl, J. D. Yakobi-Hancock, J. P. D. Abbatt, J. Y. Aller, A. K. Bertram, D. A. Knopf, and B. J. Murray (2015), A marine biogenic source of atmospheric ice-nucleating particles, *Nature*, *525*, 234–238.

Winker, D. M., M. A. Vaughan, A. Omar, Y. Hu, K. Powell, Z. Liu, W. H. Hunt, and S. A. Young (2009), Overview of the CALIPSO mission and CALIOP data processing algorithms, *J. Atm. Ocean. Tech.*, *26*(11), 2310–2323.

Zelinka, M. D., S. A. Klein, and D. L. Hartmann (2012), Computing and partitioning cloud feedbacks using cloud property histograms. part II: Attribution to changes in cloud amount, altitude, and optical depth, *J. Clim.*, *25*(3736–3754).